PCCP

Infrared Photodissociation Spectroscopy of Di-Manganese Oxide Cluster Cations

Journal:	*Physical Chemistry Chemical Physics*
Manuscript ID	CP-ART-08-2019-004586.R1
Article Type:	Paper
Date Submitted by the Author:	11-Oct-2019

Complete List of Authors:	Zimmermann, Nina; Ulm University, Institute of Surface Chemistry and Catalysis Bernhardt, Thorsten; Ulm University, Institute of Surface Chemistry and Catalysis Bakker, Joost; Radboud Universiteit Faculteit der Natuurwetenschappen Wiskunde en Informatica Landman, Uzi; Georgia Institute of Technology, School of Physics Lang, Sandra; Ulm University, Institute of Surface Chemistry and Catalysis

Physical Chemistry Chemical Physics

ARTICLE

Infrared Photodissociation Spectroscopy of Di-Manganese Oxide Cluster Cations

Received 00th January 20xx,
Accepted 00th January 20xx

DOI: 10.1039/x0xx00000x

Nina Zimmermann,[a] Thorsten M. Bernhardt,[a] Joost M. Bakker,[b] Uzi Landman,[c] Sandra M. Lang[a]*

Infrared multiple-photon dissociation (IR-MPD) spectroscopy and density functional theory (DFT) calculations have been employed to elucidate the geometric structure of a series of di-manganese oxide clusters $Mn_2O_x^+$ (x = 4-7). The theoretical exploration predicts that all investigated clusters contain a rhombus-like Mn_2O_2 core with up to four, terminally bound, oxygen atoms. The short Mn-O bond length of the terminal oxygen atoms of ≤ 1.58 Å indicates triple bond character instead of oxyl radical formation. However, the IR-MPD spectra reveal that higher energy isomers with up to two O_2 molecules η^2-coordinated to the cluster core can be kinetically trapped under the given experimental conditions. In these complexes, all O_2 units are activated to superoxide species. In addition, the sequential increase of the oxygen content in the cluster allows for a controlled increase of the positive charge localized on the Mn atoms reaching a maximum for $Mn_2O_7^+$.

1 Introduction

The design of cost and energy efficient water oxidation catalysts represents one of the most important challenges of current catalysis research. In nature, the oxidation of water is catalyzed by an inorganic calcium-manganese oxide cluster ($CaMn_4O_5$) which is embedded in the protein structure of photosystem II.[1] Inspired by this biological catalyst consisting of earth-abundant and thus cheap elements, extensive research efforts have been invested in the synthesis of manganese based model complexes serving as functional synthetic analogues of the natural cluster complex. During the last decades the synthesis of mono-, di-, tri-, and tetra-nuclear manganese complexes have been reported. Due to their structural relevance, complexes with a rhombus-like $Mn_2(\mu_2\text{-}O)_2$ core, the "butterfly" structure with a $Mn_4(\mu_2\text{-}O)_2$ core as well as complexes containing Mn_4O_4 cores of different geometry, such as, e.g., the "dimer-of-dimers" (two connected $Mn_2(\mu_2\text{-}O)_2$ units) and the cubic $Mn_4(\mu_3\text{-}O)_4$ structure, are probably the most famous clusters among the multitude of different reported species. Synthesis routes, geometric details, and physical-chemical properties of numerous synthetic molecular model complexes have been summarized in several comprehensive review articles.[2,3,4]

In the natural system the $CaMn_4O_5$ cluster is known to cycle through a series of five different oxidation states, the S_n (n = 0 - 4) states, and as soon as the S_4 state is reached molecular oxygen, O_2, is released and the S_0 state is regenerated.[5] Thus, much effort has not only been devoted to the synthesis of manganese-oxide clusters with different nuclearity, but also with Mn atoms of different oxidation states and in particular to the synthesis of high-valent Mn-oxo species.[3] For the formation and stabilization of high-valent manganese-oxide clusters the choice of ligands plays an important role and complexes with a great variety of different ligands have been reported.[3,4]

Besides changing the manganese oxidation state by appropriate ligands, the formal Mn oxidation state can also be tuned by variation of the Mn/O ratio. However, this approach is rarely pursued in synthetic chemistry. While a few non-stoichiometric oxygen-rich tri- and tetra-nuclear clusters such as Mn_3O_4, Mn_4O_5, and Mn_4O_6 have been synthesized[3,4] there are only two examples for oxygen-rich di-nuclear clusters in the literature: a complex with a $Mn_2(\mu_2\text{-}O)_3$ core, and a complex with a $Mn_2(\mu_2\text{-}O)_2(\mu_2\text{-}O_2)$ core containing a peroxo bridge.[6,7]

In this contribution, we report on the preparation of a series of cationic di-manganese-oxide clusters $Mn_2O_x^+$ with up to seven oxygen atoms, via laser ablation of a manganese target in the presence of O_2 diluted in a helium buffer gas. Density functional theory (DFT) calculation reveal that all these clusters contain in the lowest energy configuration a rhombus-like Mn_2O_2 core similar to the previously synthesized complexes, and bind up to four oxygen atom as terminal manganyl Mn-O groups. Further oxygen is then bound molecularly. In contrast, infrared multiple-photon dissociation (IR-MPD) spectroscopy indicates that the prepared complexes contain up to two η^2-bound O_2 units and only clusters with an odd number (x) of oxygen atoms contain a manganyl group. Transition state calculations suggest that the larger Mn_2O_x (x = 4-7) clusters are formed from adsorption of O_2 onto Mn_2O_x (x = 2,3) and that they are kinetically trapped under the current experimental conditions. Although IR-MPD spectroscopy represents a powerful tool for structural characterization it does not provide direct information on oxidation states and charge distributions

[a] Institute of Surface Chemistry and Catalysis, University of Ulm, Albert-Einstein-Allee 47, 89069 Ulm, Germany
[b] Radboud University, Institute for Molecules and Materials, FELIX Laboratory, Toernooiveld 7, 6525 ED Nijmegen, The Netherlands
[c] School of Physics, Georgia Institute of Technology, Atlanta, GA 30332-0430, USA

Electronic Supplementary Information (ESI) available: See DOI: 10.1039/x0xx00000x

within the cluster. To obtain such information for gas-phase species, alternative experimental methods such X-ray absorption spectroscopy are more suitable (see e.g. Ref. [8]). Nevertheless, a theoretical charge analysis of the clusters studies in the present work, shows that the sequential attachment of oxygen to the Mn_2O_2 core allows for a controlled change of the charge of the Mn atoms, reaching a maximum of 2.19e for $Mn_2O_7^+$.

2 Methods

2.1 Experimental Methods

Cationic manganese oxide clusters were produced by pulsed laser ablation of a rotating manganese rod using the second harmonic of a Nd:YAG laser. The ablation took place in a 3 mm diameter and 60 mm long growth channel in the presence of a short pulse of helium carrier gas seeded with 0.06% O_2. The manganese-oxygen-helium mixture was expanded into vacuum forming a molecular beam before entering the intracavity region, where it interacted with the IR laser beam of the Free Electron Laser for Intra Cavity Experiments (FELICE, 240–1500 cm-1; 10 μs pulse duration; spectral width approximately 0.4% FWHM of the central frequency), crossing it at an angle of 35°. A few μs after the interaction with FELICE, all clusters were extracted by a set of pulsed high voltage plates into a reflectron time-of-flight mass spectrometer and detected with a microchannel plate detector.[9] To correct for long term source fluctuations, the experiment was operated at twice the FELICE repetition rate, allowing for the recording of reference mass spectra in between successive FELICE pulses. Whenever FELICE was in resonance with an IR active vibrational mode of a given cluster, multiple IR photons were absorbed sequentially, leading to the heating of the complex and finally to its fragmentation.

The IR-MPD spectra shown in this contribution display the ratio of the mass peak intensity obtained with (I) and without (I_0) laser light. When the light is not resonant with a vibrational transition, no fragmentation occurs, and the ratio I/I_0 is 1. In case of resonant absorption of IR light, the cluster complex fragments and the ratio I/I_0 becomes smaller than 1 (signal depletion). At the same time a larger cluster may fragment into the mass channel of a specific cluster complex, causing an intensity gain, which is reflected by a I/I_0 value larger than 1. The sequential fragmentation can, in some cases, lead to the overlap of signal depletion and gain and thus, influence the peak shape or the signal intensity. This implies that the depletion yield presented here, which is strictly speaking not the same as the IR intensities calculated, cannot be quantitatively compared; however, there should be a correlation between the depth of the depletion and the calculated IR intensity. The drawback arising from the nonexistence of mass-selection prior to IR irradiation is, however, offset by the possibility to simultaneously record IR spectral signatures for multiple cluster sizes, providing an internal frequency calibration.

2.2 Theoretical Methods

The theoretical exploration of the di-manganese oxide clusters was performed with the use of density-functional theory (DFT) employing the Vienna ab initio simulation package VASP.[10] The wavefunctions were expanded in a plane wave basis with a kinetic energy cut-off of 400 eV. The interaction between the atom cores and the valence electrons was described by the projector augmented-wave (PAW) potential[11] and the exchange-correlation functional was described by the PBE generalized gradient approximation (GGA).[12]

For all calculations, a supercell with a lattice constant of 25 Å was used to avoid any interactions between the cluster complexes and their periodic images. To further minimize the electrostatic interaction with the images a neutralizing background charge as well as dipole and quadrupole corrections to the total energy were applied for cationic clusters.[13] For structure optimization, convergence was achieved when the change in the total free energy was smaller than 10^{-6} eV. In the following, we denote the difference between the number of majority and minority spin electrons (spin-up and spin-down electrons) by $\mu = N\uparrow - N\downarrow$.

The vibrational spectra of the cluster complexes were calculated in the harmonic approximation by determining the dynamical matrix (matrix containing the electron density response to atomic displacements from equilibrium) using density functional perturbation theory.[14]

3 Results and Discussion

3.1 Determination of Frequency Scaling Factors

In our previous IR-MPD spectroscopic studies of manganese oxide clusters, we mainly focused on the activation of adsorbed water molecules by probing the water bending mode.[15,16] In this spectral region the agreement between the theoretical predicted vibrations and the experimental found modes was satisfactorily and thus, the introduction of frequency scaling factors to account for systematic errors in the calculated vibrational frequencies and to improve the agreement with the experimental IR-MPD spectra was not necessary. For this contribution, we recorded the IR-MPD spectra of bare manganese oxide clusters for which the mismatches between the experimental and theoretical spectra appear to be larger, which makes it useful to employ frequency scaling factors. In previous spectroscopic investigations of gas phase vanadium oxide clusters two independent scaling factors have been introduced,[17,18] one for the vanadyl V-O stretch vibration and one for the remaining V-O-V and O-O modes.[17] Since our IR-MPD spectra demonstrate the preferred binding of activated but intact O_2 units (see discussion below), we have, in a first step, determined three scaling factors for: (1) the manganyl Mn-O stretch vibration, (2) the Mn-O-Mn (stretch and bending) motions of bridge

Table 1: Scaling factors and root mean square errors (rms) for different groups of vibrational frequencies obtained by a least-squares fitting procedure.[19] All vibrational modes used for the fitting procedure are given in Table S1 of the supporting information.

Mode	N[(a)]	Scaling Factor	rms/cm^{-1}
Mn-O	8	0.9002	13
Mn-O-Mn	12	0.9743	36
O-O	7	0.9806	28

[(a)] N denotes the number of vibrational modes used in the fitting procedure.

bound oxygen atoms, and (3) the O-O stretch of end-on or η^2-bound O_2.

To determine the corresponding scaling factors, a sufficiently large number of reference data is necessary. Therefore, structure optimization and vibrational frequency calculations have been performed for neutral MnO, OMnO, MnOO (with end-on bound O_2) and Mn_2O_6, for which experimental IR spectroscopic data are available in literature.[20] In addition, some of the clearly assignable modes of the presently studied clusters $Mn_2O_4^+$ and $Mn_2O_6^+$, have been used. Structural parameters of the reference systems as well as all the frequencies used here, are given in section 1 of the supporting information. Applying a least-squares fitting procedure as described in ref. 18, scaling factors of 0.9002, 0.9743, and 0.9806 with root mean square (rms) errors of 13 cm^{-1}, 36 cm^{-1}, and 18 cm^{-1} have been obtained (cf. Table 1). These values are very similar to the 0.9167 (13 cm^{-1}) and 0.9832 (26 cm^{-1}) obtained for the vanadium oxide vibrations.[17]

The scaling factors show that the Mn-O stretch is typically overestimated by about 10% (leading to a scaling factor of 0.9002), whereas the two remaining scaling factors are similar (corresponding to a theoretical frequency overestimation of about 2-3%). Due to the rather small differences of these two scaling factors (lying within the fitting error) and the fact that the exact assignment of individual modes is often difficult due to mode coupling, we will in the following only use two different scaling factors (1) a value of 0.9002 for the Mn-O stretch modes and (2) a value of 0.9743 for all other modes including Mn-O-Mn and O-O stretch vibrations.

3.2 Structure of Di-Manganese Oxide Clusters $Mn_2O_x^+$ (x = 2,3)

The laser ablation of a manganese target in the presence of 0.06% O_2 in helium leads to the formation of a series of di-manganese oxide clusters $Mn_2O_x^+$ (x = 2-7) as shown in Figure 1a. $Mn_2O_2^+$ represents the most abundant cluster in the distribution and the intensities of $Mn_2O_x^+$ (x = 3-5) are about four times smaller. The larger clusters $Mn_2O_6^+$ and $Mn_2O_7^+$ are only produced in small amounts (the mass signal intensity is about 8-10 times lower than for $Mn_2O_2^+$). Using a similar laser ablation technique Koyama et al. previously reported the production of only larger manganese oxide clusters with three and more Mn atoms.[21] In contrast, cluster formation in a gas aggregation source[22] as well as a CORDIS sputter source[23] also resulted in the preferred formation of $Mn_2O_2^+$.

Despite the high abundance of $Mn_2O_2^+$ and $Mn_2O_3^+$ in the molecular beam, it was under the current experimental

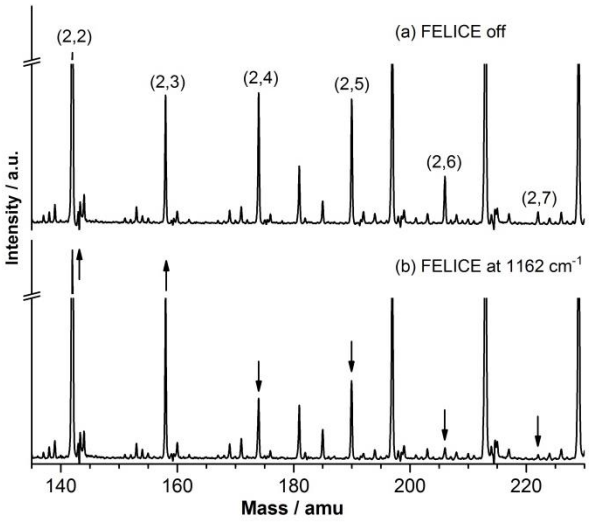

Figure 1: Cluster distribution obtained (a) without and (b) with IR light at 1162 cm^{-1} in the size range of $Mn_2O_2^+$ to $Mn_2O_7^+$. The arrows indicate signal gain (up) or depletion (down) upon interaction with the IR light. The unlabeled mass peaks correspond mainly to manganese-oxide clusters of different nuclearity which are simultaneously produced in the cluster source as well as to complexes arising from water contaminations.

conditions not possible to obtain IR-MPD spectra of these clusters. Figure 1b displays a representative mass spectrum obtained after IR irradiation of the cluster beam at 1162 cm^{-1}, clearly showing a signal depletion on the masses of $Mn_2O_{4-7}^+$ (indicated by a downward pointing arrow) and a signal gain on the masses of $Mn_2O_2^+$ and $Mn_2O_3^+$ (indicated by an upward pointing arrow) compared to the spectrum in Figure 1a. This shows that the latter clusters represent the fragmentation products of the larger oxides with $x > 3$. Accordingly, their IR-MPD spectra are dominated by signal gain ($I/I_0 > 0$) in the whole investigated spectral region. The lack of any depletion signals ($I/I_0 < 1$) most likely arises from the high stability of these clusters which prevents their fragmentation upon absorption of IR light.

Previous DFT calculations suggested that cationic $Mn_2O_2^+$ has a rhombus-like structure[24] similar to the structure predicted for neutral Mn_2O_2[24,25] as well as to the structure of synthesized complexes with an $Mn_2(\mu_2\text{-}O)_2$ core.[3] In the current work, the lowest energy $Mn_2O_2^+$ isomer was again found to be rhombus-like and having the highest possible spin configuration of $\mu = 9$ unpaired electrons (which corresponds to a spin multiplicity 2S+1 = 10). According to a Bader charge analysis[26] a positive charge of Δq = +1.49e and +1.48e (cf. Table 2), respectively, is located on the Mn atoms, although the formal oxidation state of this structure is Mn(2.5)-Mn(2.5). All other spin isomers are considerably (> 1 eV) higher in energy.

For $Mn_2O_3^+$, not previously addressed, we find several energetically low lying isomers. In the lowest energy structure ($\mu = 1$, iso 2,3-a, cf. Figure S1 of the supporting information), the additional oxygen atom binds to one of the Mn atoms with an angle α of 138° relative to the rhombic Mn_2O_2 plane forming a manganyl-oxide unit ($Mn_2(\mu_2\text{-}O)_2O$). This structure corresponds to formal oxidation states of Mn(4.5)-Mn(2.5),

Table 2: Positive charge Δq localized on the Mn atoms (labeled Mn1 and Mn2) obtained by Bader charge analysis.[26]

Cluster	isomer	Δq(Mn1)	Δq(Mn2)
$Mn_2O_2^+$	iso 2,2-a(9)	+1.49e	+1.48e
$Mn_2O_3^+$	iso 2,3-a(1)	+1.86e	+1.64e
$Mn_2O_4^+$	iso 2,4-a (1)	+1.70e	+1.57e
$Mn_2O_5^+$	iso 2,5-a(1)	+2.05e	+1.76e
$Mn_2O_6^+$	iso 2,6-a(1)	+1.85e	+1.75e
$Mn_2O_7^+$	iso 2,7-a(3)	+2.19e	+2.13e

whereas Bader charge analysis reveals an increase of the excess charge located on the O binding and non-binding Mn atom to +1.86e and +1.64e, respectively, and a negative charge of -0.65e localized on the terminal O atom. Further analysis of the spin density difference (i.e. difference of up and down spin density, cf. Figure S1) shows that most of the excess spin is localized on the Mn atoms showing the formation of a manganyl Mn=O or Mn≡O group instead of an oxyl Mn-O· radical. This is consistent with a short Mn-O bond length of 1.58 Å indicating triple bond character[4] as, e.g., also observed for early first row transition metal oxides.[27]

A 2D isomer with α = 180° (μ = 3, iso 2,3-b) is only 0.1 eV higher in energy and a 3D isomer with α = 132° (μ = 7, iso 2,3-c) is 0.21 eV less stable. All structures with three bridging oxygen atoms (iso 2,3-d, $Mn_2(\mu_2\text{-}O)_3$) or a bridging O_2 unit (iso 2,3-e, $Mn_2(\mu_2\text{-}O)(\mu_2\text{-}O_2)$) are more than 1.80 eV higher in energy. Interestingly, in the presence of appropriate ligands, a $Mn_2(\mu_2\text{-}O)_3$ structure has previously been shown to be stable.[7] A similar minimum energy structure has previously also been found for neutral Mn_2O_3 with the $Mn_2(\mu_2\text{-}O)_3$ structure being 0.93 eV less stable.[28]

3.3 IR-MPD Spectra of $Mn_2O_x^+$ (*x* = 4,6)

Figure 2 displays the IR-MPD spectra of the di-manganese oxide clusters with four (left column) and six (right column) oxygen atoms together with the calculated spectra of three isomeric structures. The spectrum of $Mn_2O_4^+$ shows three bands centered at 1157 cm^{-1} (I), around 670 cm^{-1} (II, with peaks at 719, 692, and 652 cm^{-1}), and at 446 cm^{-1} (III) as well as the onset of a band at the red edge of the spectrum. Band I is characteristic for the O-O stretch mode of a superoxide species[29] indicating the presence of an activated but intact O_2 unit. Furthermore, the gain signals observed in the $Mn_2O_2^+$ mass channel are, to a large extent, consistent with the depletion signals of $Mn_2O_4^+$ indicating the fragmentation of $Mn_2O_4^+$ via loss of an O_2 molecule upon resonant absorption of IR light.

$$Mn_2O_4^+ + n\text{hv} \rightarrow Mn_2O_2^+ + O_2$$

A similar fragmentation process via loss of O_2 has previously also been observed for complexes of $Mn_2O_4^+$ with water $Mn_2O_4(H_2O)_n^+$.[16] Bands where I/I_0 exceeds 1 are consistent with a similar fragmentation process when irradiating $Mn_2O_6^+$, see below.

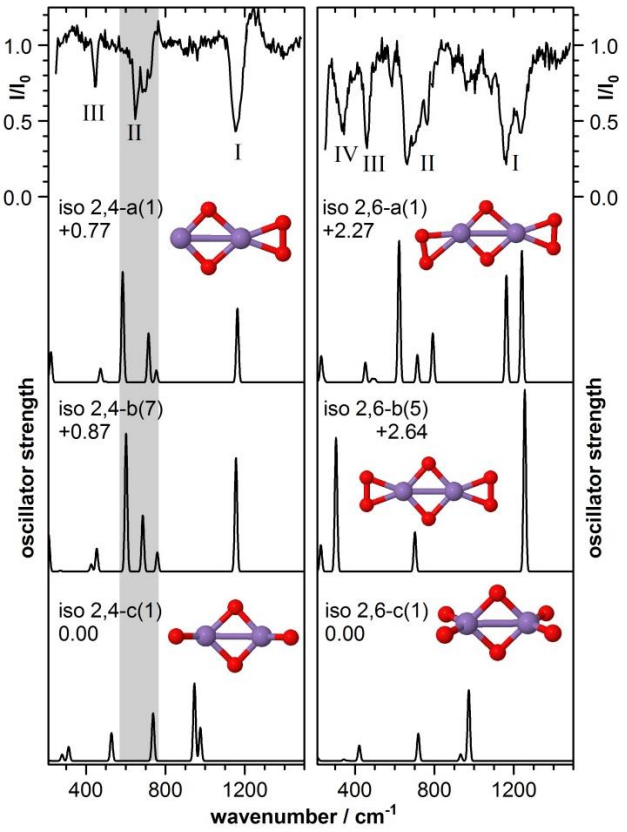

Figure 2: IR-MPD spectra of $Mn_2O_4^+$ (left column) and $Mn_2O_6^+$ (right column) together with the calculated vibrational spectra of three isomeric structures. The theoretical spectra are obtained by convolution of the oscillator strength with a 20 cm^{-1} FWHM Gaussian line shape function. The gray shaded area is shown to guide the eye. Also given are the relative energies in eV and the number of unpaired electrons μ (in brackets). Mn and O atoms are depicted as purple and red spheres, respectively, Geometric details are provided in Figure S2 and S3.

The tentative assignment of the spectrum to an $Mn_2O_2^+$ core with an activated molecular O_2 adduct can be verified by the calculated vibrational spectra of $Mn_2O_4^+$ which will be discussed in the following. The second trace of Figure 2 (left column) displays the calculated spectrum of isomer iso 2,4-a (μ = 1) comprising a rhombus-like Mn_2O_2 core and an oxygen molecule η^2-bound to one of the Mn atoms (geometric details are given in Figure S2). Attachment of an O_2 unit instead of an oxygen atom (as in $Mn_2O_3^+$) leads to a smaller excess positive charge on the Mn atoms of +1.70e and +1.57e, respectively. The overall features of this spectrum are consistent with the IR-MPD spectrum of $Mn_2O_4^+$. Based on this spectrum, band I can indeed be assigned to the O-O stretch motion of a superoxide species with an O-O distance of 1.33 Å (calculated at 1162 cm^{-1}), the broad and structured band II is assigned to three modes corresponding to motions of the Mn_2O_2 core (calculated at 754, 715, and 585 cm^{-1}) as well as band III to two modes corresponding to the symmetric and asymmetric Mn-O_2 stretch (coupled with Mn-O-Mn modes, 476 and 471 cm^{-1}). While the general agreement between calculated and experimental spectrum is quite reasonable, the calculated values of 754, 715

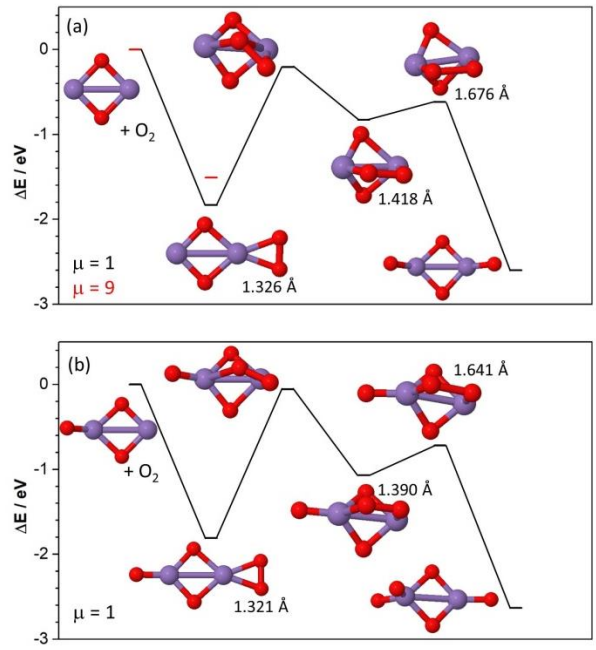

Figure 3: (a) Calculated reaction pathway for the adsorption of O_2 on $Mn_2O_2^+$ leading to $Mn_2O_4^+$ (iso 2,4-a) and subsequent dissociation of O_2 resulting in iso 2,4-c. (b) Reaction pathway for the adsorption of O_2 on $Mn_2O_3^+$ leading to $Mn_2O_5^+$ (iso 2,5-a) and subsequent dissociation of O_2 resulting in iso 2,5-c. Mn and O atoms are depicted as purple and red spheres, respectively. The numbers given next to the structures denote the O-O bond length. The excess spin number (μ, see section 2.2) is noted in each panel.

and 476/471 cm^{-1} are (after scaling) blue-shifted by about 30 cm^{-1} compared to the experimental spectrum, while the most prominent of the predicted modes responsible for band II, calculated at 585 cm^{-1}, is red-shifted by about 70 cm^{-1}. A somewhat better agreement between the theoretical and experimental spectrum is achieved for the spin isomer with μ = 7 unpaired electrons (iso 2,4-b, third trace in Figure 2, left column) which is calculated to be only 0.10 eV higher in energy. For this isomer, the modes of the Mn_2O_2 core are at 759, 686, and 602 cm^{-1} giving perhaps a better match for the two most intense features of band II (for better visibility this area is highlighted in gray) and the Mn-O_2 stretch modes are at 453 and 426 cm^{-1}, respectively, providing a slightly better match for the more intense mode of the two with band III. For both spin isomers the onset of a further band at the red edge of the IR-MPD spectrum can be explained by the out of plane Mn-O-Mn bending motion of the Mn_2O_2 cluster core (calculated at 223 cm^{-1} for μ = 1 and at 212 cm^{-1} for μ = 7 isomer).

Although all features of the IR-MPD spectrum can thus be rather well accounted for by an isomer with molecularly bound O_2, isomers 2,4-a and 2,4-b do not represent the minimum energy structure: an isomer containing two manganyl units (isomer 2,4-c, μ = 1, bottom trace of Figure 2, left column; geometric details in Figure S2) is 0.77 eV lower in energy than iso 2,4-a. A similar structure has also been predicted for neutral Mn_2O_4 by DFT calculations.[30] However, it is clear that the calculated spectrum strongly disagrees with the IR-MPD spectrum of $Mn_2O_4^+$. Potentially, one could argue that the small structure in the experimental spectrum just below 1000 cm^{-1} is a signature of the presence of iso 2,4-c, but all evidence indicates that the higher energy isomer containing an oxygen molecule is kinetically trapped under the given experimental conditions and the minimum energy structure is not, or only marginally, formed. This trapping of the higher energy isomer can be explained by the rather high energy barrier associated with the dissociation of adsorbed O_2 (cf. Figure 3a): The energy difference between $Mn_2O_4^+$ (μ = 1) relative to $Mn_2O_2^+$ (μ = 9) and O_2 is -1.83 eV. Dissociation of the O_2 molecule proceeds via bridging of the O_2 molecule between the two Mn atoms (leading to the elongation of the O-O bond from 1.326 Å in iso 2,-4-a to 1.418 Å) followed by an O-O bond rupture. These reaction steps are calculated to require an energy of +1.62 eV and +0.22 eV, respectively. Thus, the energy required to overcome the first barrier (1.62 eV) is only slightly lower than the energy gained upon O_2 adsorption (-1.83 eV) which makes the O_2 dissociation reaction slow and most likely leads to the trapping of iso 2,4-a.

The IR-MPD spectrum recorded for the mass channel of $Mn_2O_6^+$ (right column of Figure 2) is more congested than that for $Mn_2O_4^+$, but nevertheless shows great similarity to it in showing depletions at largely the same frequencies for bands I, II, and III as well as the onset of a band at the red edge of the spectrum. One clear additional band centered at 336 cm^{-1} (labeled IV) is observed in the spectrum of $Mn_2O_6^+$. Despite the similarity in the spectra, an important difference is found for band I: for $Mn_2O_6^+$ band I clearly consists of two partially overlapping modes, indicating the likely presence two intact O_2 molecules. The similarity of the spectra and the double peak structure of band I suggests that $Mn_2O_6^+$ is formed via attachment of an O_2 molecule to $Mn_2O_4^+$, giving a structure with two differently bound O_2. This spectrum is largely consistent with a reported IR-MPD spectrum of $Mn_2O_6^+$ obtained with the less intense IR light of the free electron laser FELIX.[31] However, in that spectrum band III only appears with very low intensity and band IV is missing.

Indeed, the majority of features in the IR-MPD spectrum, except for band IV, can be satisfactorily explained by the calculated vibrational spectrum of a structure (iso 2,6-a, μ = 1) which is formed via η^2-binding of a second O_2 molecule to the initially unoccupied Mn atom of $Mn_2O_4^+$. This additional O_2 further increases the charge localized on the Mn atoms to +1.75e/+1.85e. Furthermore, the second O_2 molecule is tilted with respect to the Mn_2O_2 core giving rise to two different frequencies of the O-O stretch mode (1240 cm^{-1} and 1162 cm^{-1}) in agreement with the double peak structure of band I (geometric details of this structure are given in Figure S3 of the supporting information).

A second, more symmetric isomer (iso 2,6-b, μ = 5) is found to be 0.35 eV higher in energy. Due to its symmetry, the calculated spectrum (third panel in Figure 2, right column) only shows three clearly separated modes. The first mode at 1255 cm^{-1} corresponds to the asymmetrically coupled O-O stretch mode of both O_2 molecules and the other two modes at 702 cm^{-1} and 304 cm^{-1} correspond to symmetric motions of the Mn_2O_2 core. All other vibrations in the investigated spectral region are calculated to have very low oscillator strength and are thus not visible in the spectrum. The modes at 1255 cm^{-1} and 702 cm^{-1}

are in agreement with bands I and II of the IR-MPD spectrum and cannot be distinguished from the corresponding modes of iso 2,6-a. In contrast, the mode at 304 cm^{-1} is unique for iso 2,6-b and can explain the occurrence of band IV centered at 336 cm^{-1}, suggesting that this isomer is also present in the molecular beam.

Similar to the situation for $Mn_2O_4^+$, both iso 2,6-a and iso 2,6-b containing two η^2-coordinated O_2 units do not represent the lowest energy structures. The lowest energy structure (iso 2,6-c, bottom trace of Figure 2 and Figure S3) is a symmetric structure with four oxygen atoms terminally bound to the Mn_2O_2 core. This isomer is with 2.27 eV considerably more stable than iso 2,6-a. The high stability of the manganyl group containing structure is caused by the reduced binding energy of the second O_2 of only 1.20 eV (compare to 1.83 eV for the first O_2, cf. Figure 3a). The corresponding vibrational spectrum shown in Figure 2 exhibits three dominant modes which again cannot explain the major features observed in the IR-MPD spectrum. It appears that this isomer might form a minor contribution to the spectrum evidenced from a weak signal coinciding with the most intense band predicted at 973 cm^{-1}. A further isomer (iso 2,6-d, Figure S3) with one η^2-bound O_2 and two manganyl groups is 1.42 eV higher in energy than iso 2,6-c but its existence can be excluded on basis of the IR-MPD spectrum.

Thus, we conclude that all features of the $Mn_2O_6^+$ IR-MPD spectrum can be satisfactorily explained by the co-existence of two isomeric structures, the asymmetric structure iso 2,6-a, and the highly symmetric structure iso 2,6-b. Both structures are formed by attachment of two O_2 molecules to the near-rhombic $Mn_2O_2^+$ and are considerably higher in energy than the minimum energy structure. This shows again that under the experimental conditions of the laser vaporization source the isomers with intact O_2 units can be kinetically trapped.

3.4 IR-MPD Spectra of $Mn_2O_x^+$ (x = 5,7)

Figure 4 displays the IR-MPD spectra of $Mn_2O_5^+$ and $Mn_2O_7^+$ together with the calculated spectra of three isomeric structures. Similar to the spectra for $Mn_2O_4^+$ and $Mn_2O_6^+$, the spectra for the clusters containing an odd number of oxygen atoms (odd x) show a band around 1200 cm^{-1}, characteristic for a superoxide species, as well as one around 450 cm^{-1} which has above been found to mainly arise from coupled Mn-O_2 stretch motions. However, in the spectral region between 1200 and 450 cm^{-1} the spectra of the odd x clusters are considerably different from those of the even x clusters.

The IR-MPD spectrum of $Mn_2O_5^+$ (left column of Figure 4) shows six bands centered at 1190 (I), 977 (II), 760 (III), 603 (IV), 428 (V), and 267 cm^{-1} (VI), respectively. The signal depletions of $Mn_2O_5^+$ are clearly reflected as signal gains in the mass channel of $Mn_2O_3^+$ giving evidence for the fragmentation of $Mn_2O_5^+$ into $Mn_2O_3^+$ via loss of O_2 upon absorption of IR light

$$Mn_2O_5^+ + n\text{hv} \rightarrow Mn_2O_3^+ + O_2$$

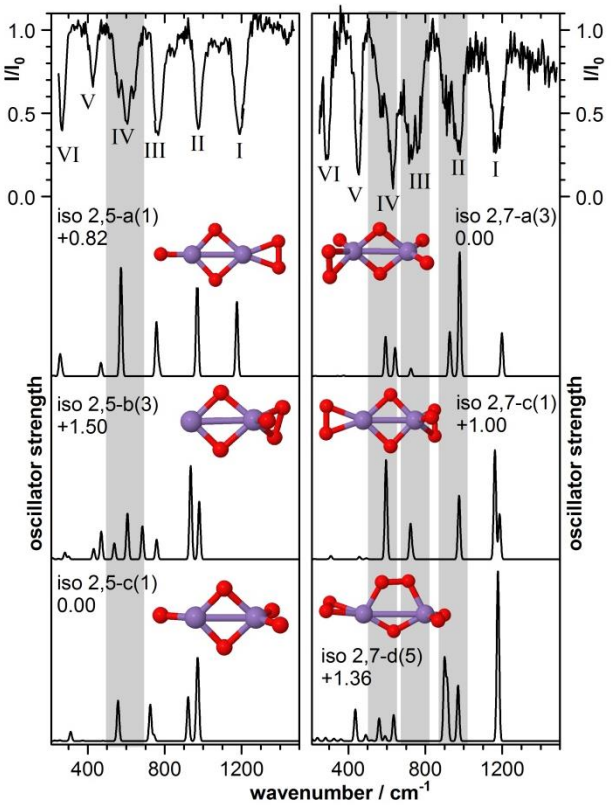

Figure 4: IR-MPD spectra of $Mn_2O_5^+$ (left column) and $Mn_2O_7^+$ (right column) together with the calculated vibrational spectra of three isomeric structures. The theoretical spectra are obtained by convolution of the oscillator strength with a 20 cm^{-1} FWHM Gaussian line shape function. Also given are the relative energies in eV and the numbers in brackets denote the number of unpaired electrons (μ). The gray shaded areas are shown to guide the eye. Mn and O atoms are depicted as purple and red spheres, respectively, Geometric details are provided in Figure S4 and S5.

This fragmentation channel together with the observation of the characteristic O-O stretch mode of a superoxide species at 1190 cm^{-1} again indicates the existence of an intact O_2. All features of the IR-MPD spectrum, except for band V have also previously been observed using the IR light provided by FELIX.[31]

The lowest energy structure of $Mn_2O_5^+$ containing a superoxide species can be regarded as an $Mn_2O_3^+$ cluster with an O_2 unit η^2-bound to the second Mn atom (the one not binding the terminal O) and has μ = 1 unpaired electrons (iso 2,5-a, α = 173°, d(Mn-O) = 1.57 Å, charge of +1.76e/+2.05e on the Mn atoms; cf Figures 4 and S4). The calculated vibrational spectrum of this isomer (second trace of Figure 4, left column) shows six bands and accounts for all features observed in the IR-MPD spectrum. Based on this spectrum, band I is assigned to the O-O stretch motion of the O_2 unit (calculated at 1175 cm^{-1}), band II to the Mn-O stretch motion of the manganyl group (969 cm^{-1}), bands III, IV, and VI to modes of the Mn_2O_2 core (770, 757, 572, and 255 cm^{-1}), and band V to the symmetric Mn-O_2 stretch motion (coupled with Mn-O-Mn motions, 468 cm^{-1}), respectively. While the calculated modes are in good agreement with bands I, II, III, and VI, the calculated value for band IV is red-shifted by about 30 cm^{-1} and the calculated value of band V is blue-shifted by 40 cm^{-1}. The red-shift of band IV is

consistent with the red-shift of the mode predicted for band II around 600 cm^{-1} in the spectra of both $Mn_2O_4^+$ and $Mn_2O_6^+$.

Band IV of $Mn_2O_5^+$ is slightly broader than the other bands, and it contains substructure, suggesting the overlap of at least three modes. Since iso 2,5-a has only one vibration in this spectral region (at 572 cm^{-1}) this broadening could indicate the co-existence of a further isomer. Spin isomers are found to be 0.29 eV (μ = 5), 0.52 eV (μ = 7), and 0.60 eV (μ = 3) higher in energy. Due to the similar geometry (details are given in Figure S4) of these isomers to iso 2,5-a, the overall vibrational spectra are also very similar and the individual modes are only slightly red- or blue-shifted depending on the spin state. Thus, the co-existence of one (or more) of these spin isomers cannot be excluded and might contribute to the broadening of band IV.

Besides these spin isomers, further geometrical isomers have also been found. One possible geometry consists of a near-rhombic Mn_2O_2 core with the O_2 molecule and the oxygen atom bound to the same Mn atom. The energetically lowest spin isomer of this geometry has μ = 3 unpaired electrons (iso 2,5-b) and is 0.68 eV higher in energy than iso 2,5-a. The corresponding vibrational spectrum is shown in the third trace of Figure 4, left column. This spectrum shows a series of six peaks between 400 and 800 cm^{-1}. Some of the modes predicted are consistent with the observed spectrum (notably for bands III-V); however, the intense double peak around 950 cm^{-1} (arising from the O-O and the Mn-O stretch modes) should lead to a broadening of band II if this isomer were present in substantial amounts, which is not clearly observed in the IR-MPD spectrum.

As already observed for the even *x* $Mn_2O_x^+$ clusters, isomers containing a superoxide species do not represent the lowest energy structures. Isomer 2,5-c with three manganyl groups is 0.82 eV more stable than iso 2,5-a. The corresponding calculated vibrational spectrum (Figure 4, left column, lowest panel) might account for band III (although the calculated mode is red-shifted by about 35 cm^{-1}), and parts of band IV, and VI, but clearly not for bands I and V. The co-existence of iso 2,5-c cannot be completely excluded, but is expected to be minimal, based on similar grounds for ruling out the substantial presence of iso 2,5-b in that it should be evidenced from a clear broadening of band II which is not observed. Thus, it can be concluded that the IR-MPD spectrum of $Mn_2O_5^+$ is well explained by the dominant presence of iso 2,5-a, except for the broadened and structured band IV. Contributions from one or more spin isomers leading to this broadening is very likely although a clear assignment is not possible.

Similar to the above discussed $Mn_2O_4^+$ the trapping of the higher energy isomer 2,5-a can be explained by the rather high energy barrier associated with the dissociation of O_2 (cf. Figure 3b). In this case, the binding energy between $Mn_2O_3^+$ and O_2 amounts to 1.81 eV and the barriers encounter for O_2 dissociation (proceeding via an intermediate with the O_2 unit bridged between the two Mn atoms) are calculated to amount to 1.75 eV and 0.35 eV, respectively. These energetics make the O_2 dissociation very slow and most likely lead to the trapping of iso 2,5-a.

Finally, the right column of Figure 4 displays the IR-MPD spectrum of $Mn_2O_7^+$ which shows six bands centered at 1172 cm^{-1} (I), 969 cm^{-1} (II), around 740 cm^{-1} (III), 630 cm^{-1} (IV), 452 cm^{-1} (V), and 287 cm^{-1} (VI). This spectrum is highly similar to that for $Mn_2O_5^+$, with bands I, II, and III at near-identical frequencies. Both II and III now have a sideband at lower frequency, for III it is the dominant component. Bands IV and VI now have a stronger high-frequency component, and band V is outright blue-shifted.

The similarity between the IR-MPD spectra of $Mn_2O_7^+$ and $Mn_2O_5^+$ indicates a similar structural motif for both clusters. However, the theoretical exploration of the $Mn_2O_7^+$ cluster geometry appears to be considerably more complex than for the smaller clusters. $Mn_2O_7^+$ represents the first cluster studied here, for which the geometry containing the maximum number of manganyl groups (in this case five) does not represent the minimum energy structure (+2.69 eV higher in energy than the found lowest energy structure). Two energetically low lying structures containing three manganyl groups and one O_2 have been found. Iso 2,7-a (μ = 3, charge of +2.13e on the Mn atom binding O/O_2 and 2.19e on the Mn atom binding 2O; cf. Figures 4 and S5) represents the lowest energy structure and contains a η^2-bound superoxide species (*d*(O-O) = 1.31 Å), whereas iso 2,7-b (μ = 3, +0.27 eV, Figure S5) contains η^1-bound di-oxygen (d(O-O) = 1.25 Å). The calculated vibrational spectrum of iso 2,7-a, shown in the second panel of Figure 4 (right column) could account for the experimentally observed bands I to IV. In particular, it offers an explanation for the extra structure of bands II and IV. However, it exhibits no sideband of band III and more importantly, the vibrations in the spectral region below 500 cm^{-1} are calculated to be very weak, in disagreement with the strong bands V and VI. η^1-binding of di-oxygen in iso 2,7-b considerably blue-shifts the O-O to 1344 cm^{-1} which is not observed in the IR-MPD spectrum and makes us exclude the co-existence of this isomer.

All found isomers containing only one manganyl group besides two O_2 units are at least 1.00 eV less stable, however, we have shown above that kinetically trapping of such structures is possible and must consequently be considered for $Mn_2O_7^+$. The lowest energy geometry of $Mn_2O_7^+$ containing two O_2 units (iso 2,7-c) can be regarded as iso 2,5-a with a second O_2 molecule η^2 bound to the same Mn atom as the terminal O atom. This leads to the rotation of the terminal oxygen resulting in an angle α of 118° relative to the rhombic Mn_2O_2 plane. The attachment of seven oxygen atoms to the Mn_2O_2 core results in the highest positive charge localized on the Mn atoms of +1.78e/+2.12e of all the experimentally found structures. The most stable spin state corresponds to μ = 1 unpaired electron (iso 2,7-c, +1.00 eV), while the μ = 3 and μ = 5 spin isomers are only 0.07 and 0.09 eV higher in energy, respectively (for geometric details see Figure S5). The calculated vibrational spectrum of iso 2,7-c is shown in the third panel of Figure 4 (right column) and can also account for all features observed in the IR-MPD spectrum. Bands I to IV of the IR-MPD spectrum are reproduced by the calculated spectrum, while, however, the structure of bands II, III, and IV cannot be explained. Furthermore, the intensity of bands V and VI are still strongly

underestimated in the calculations, although the intensity is increased compared to iso 2,7-a.

The spectra of the μ = 3 and μ = 5 spin isomers are very similar to the spectrum of iso 2,7-c due to the similar geometry. However, the blue-shift of the mode around 730 cm^{-1} (corresponding to a Mn-O-Mn motion of the Mn_2O_2 core) from 723 cm^{-1} for the μ = 1 isomer to 748 cm^{1} for the μ = 3 isomer, might account for the structure of band III. In contrast, the mode around 980 cm^{-1} (corresponding to the manganyl stretch) only slightly blue-shifts from 975 cm^{-1} to 981 cm^{-1} which cannot satisfactorily explain the structure of band II.

Finally, the bottom panel of Figure 4 displays the vibrational spectrum of an isomer (iso 2,7-d, +1.36 eV) containing an η^2-bound (d(O-O) = 1.32 Å) and a μ_2-bound (d(O-O) = 1.37 Å) superoxide. Also this structure can account for bands I, II, and IV and in addition has a mode at 436 cm^{-1} which is in much better agreement with band V. However, this structure also cannot account for the strong band VI. Several further isomeric structures e.g. with bridging O, rotated O_2 or both O_2 units bound to the same Mn atom were tested, and none of them was found to give an improved match with the IR-MPD spectrum. Thus, a clear structural assignment is not possible for $Mn_2O_7^+$. Several isomeric structures containing up to two O_2 units are in reasonable agreement with the IR-MPD spectrum and it is very likely that several isomeric structures (that is an isomeric mixture) contribute to this spectrum, but we cannot rule out that a further isomer not taken into account is responsible for the currently observed spectrum.

Conclusions

Synthetic manganese-oxide complexes have drawn considerable attention as functional analogues of the naturally occurring water oxidation catalysts $CaMn_4O_5$. While high-valent manganese oxide clusters are typically synthesized by the attachment of appropriate ligands, we report here on the production of a series of cationic di-manganese oxide clusters with up to seven oxygen atoms by laser ablation of a Mn target in the presence of molecule oxygen. IR-MPD spectroscopy in conjunction with DFT calculations are employed to gain insight into the geometric structure of these clusters. The theoretical investigation reveals that all clusters contain a rhombus-like Mn_2O_2 core and additional oxygen is preferably bound as manganyl groups to this core. In contrast, the IR-MPD spectra reveal the kinetic trapping of higher energy isomers containing up to two O_2 units that are η^2-bound to the Mn atoms. In all clusters, the O_2 molecule is activated to a superoxide species and only clusters with an odd number of oxygen atoms, such as $Mn_2O_3^+$, $Mn_2O_5^+$, and $Mn_2O_7^+$, contain a manganyl Mn-O unit.

The theoretically identified minimum energy structures for $Mn_2O_{2\text{-}5}^+$ containing up to three manganyl groups are similar to the previously observed structures of cationic vanadium oxide clusters.[17] However, the IR-MPD spectra of $V_2O_x^+$ did not give any indication for the kinetic trapping of the O_2-containing higher energy isomers. This could imply that the barriers for O_2 dissociation over $V_2O_2^+$ are lower than for $Mn_2O_2^+$. A further difference to the vanadium system is that the lowest energy isomer of $V_2O_6^+$ contains a η^2-superoxide as well as two manganyl groups, whereas the minimum energy structure of $Mn_2O_6^+$ is predicted to contain four manganyl groups.

Both the attachment of O_2 units and O atoms increases the positive charge localized on the Mn atoms reaching a maximum value of +2.19e for $Mn_2O_7^+$. Thus, the production and structural characterization of novel manganese oxide model systems with different oxygen content, and corresponding different Mn oxidation states (charge localized on the Mn atoms), represents an important step towards the systematic investigation of the influence of oxidation state on the water oxidation properties of di-manganese oxide clusters.

Conflicts of interest

There are no conflicts to declare.

Acknowledgements

N.Z, T.M.B, and S.M.L gratefully acknowledge support from the DFG. We also thank the Nederlandse Organisatie voor Wetenschappelijk Onderzoek (NWO) for the support of the FELIX Laboratory. The research leading to these results has received funding from LASERLAB-EUROPE (grant agreement no. 654148, European Union's Horizon 2020 research and innovation programme). Computations were carried out at the Georgia Tech Center for Computational Materials Science and U. L. was supported by grant FA9550-15-1-0519 from the U.S. Air Force Office of Scientific Research.

Notes and references

1 Y. Umena; K. Kawakami; J.-R. Shen; N. Kamiya. *Nature* 2011, **473**, 55; M. Suga; F. Akita; K. Hirata; G. Ueno; H. Murakami; Y. Nakajima; T. Shimizu; K. Yamashita; M. Yamamoto; H. Ago; J.-R. Shen. *Nature* 2015, **517**, 99.

2 M. Yagi; M. Kaneko. *Chem. Rev.* 2001, **101**, 21; R. Brimblecombe; G. C. Dismukes; G. F. Swiegers; L. Spiccia. *Dalton Trans.* 2009, 9374; G. C. Dismukes; R. Brimblecombe; G. A. N. Felton; R. S. Pryadun; J. E. Sheats; L. Spiccia; G. F. Swiegers. *Acc. Chem. Res.* 2009, **42**, 1935; M. Yagi; A. Syouji; S. Yamada; M. Komi; H. Yamazaki; S. Tajima. *Photochem. Photobiol. Sci.* 2009, **8**, 139; J. D. Blakemore; R. H. Crabtree; G. W. Brudvig. *Chem. Rev.* 2015, **115**, 12974; M. Wiechen; H.-M. Berends; P. Kurz. *Dalton Trans.* 2012, **41**, 21; M. D. Kärkäs; O. Verho; E. V. Johnston; B. Åkermark. *Chem. Rev.* 2014, **114**, 11863.

3 S. Mukhopadhyay; S. K. Mandal; S. Bhaduri; W. H. Armstrong. *Chem. Rev.* 2004, **104**, 3981.

4 C. S. Mullins; V. L. Pecoraro. *Coord. Chem. Rev.* 2008, **252**, 416.

5 B. Kok; B. Forbusch; M. McGloin. *Photochem. Photobiol.* 1970, **11**, 457.

6 U. Bossek; T. Weyhermueller; K. Wieghardt; B. Nuber; J. Weiss. *J. Am. Chem. Soc.* 1990, **112**, 6387.

7 K. Wieghardt; U. Bossek; B. Nuber; J. Weiss; J. Bonvoisin; M. Corbella; S. E. Vitols; J. J. Girerd. *J. Am. Chem. Soc.* 1988, **110**, 7398; K. Wieghardt; U. Bossek; B. Nuber; J. Weiss; S. Gehring; W. Haase. *J. Chem. Soc., Chem. Commun.* 1988, 1145.

8 L. Hirsch; J. T. Lau; P. Klar; A. Langenberg; J. Probst; J. Rittmann; M. Vogel; V. Zamudio-Bayer; T. Möller; B. v.

Issendorf. *J. Phys. B: At. Mol. Opt. Phys.* 2009, **42**, 154029; J. T. Lau; K. Hirsch; A. Langenberg; J. Probst; R. Richter; J. Rittmann; M. Vogel; V. Zamudio-Bayer; T. Möller; B. von Issendorff. *Phys. Rev. B* 2009, **79**, 241102; T. Mazza; P. Piseri; G. Bongiorno; L. Ravagnan; M. Amati; M. Devetta; C. Lenardi; M. Coreno; M. de Simone; P. Milani. *Appl. Phys. A* 2008, **92**, 463.

9 J. M. Bakker; V. J. F. Lapoutre; B. Redlich; J. Oomens; B. G. Sartakov; A. Fielicke; G. von Helden; G. Meijer; A. F. G. van der Meer. *J. Chem. Phys.* 2010, **132**, 074305; M. Haertelt; V. J. F. Lapoutre; J. M. Bakker; B. Redlich; D. J. Harding; A. Fielicke; G. Meijer. *J. Phys. Chem. Lett.* 2011, **2**, 1720.

10 G. Kresse; J. Hafner. *Phys. Rev. B* 1993, **47**, 558; G. Kresse; J. Hafner. *Phys. Rev. B* 1994, **49**, 14251; G. Kresse; J. Furthmüller. *Phys. Rev. B* 1996, **54**, 11169; G. Kresse; J. Furthmüller. *Comp. Mat. Sci.* 1996, **6**, 15.

11 G. Kresse; D. Joubert. *Phys. Rev. B* 1999, **59**, 1758.

12 J. P. Perdew; K. Burke; M. Ernzerhof. *Phys. Rev. Lett.* 1996, **77**, 3865.

13 G. Makov; M. C. Payne. *Phys. Rev. B* 1995, **51**, 4014.

14 P. Giannozzi; S. Baroni. *J. Chem. Phys.* 1994, **100**, 8537; S. Baroni; S. de Gironcoli; A. Dal Corso; P. Giannozzi. *Rev. Mod. Phys.* 2001, **73**, 515.

15 S. M. Lang; T. M. Bernhardt; D. M. Kiawi; J. M. Bakker; R. N. Barnett; U. Landman. *Angew. Chem. Int. Ed.* 2015, **127**, 15328

16 S. M. Lang; T. M. Bernhardt; D. M. Kiawi; J. M. Bakker; R. N. Barnett; U. Landman. *Phys.Chem.Chem.Phys.* 2016, **18**, 15727.

17 K. R. Asmis; G. Meijer; M. Brümmer; C. Kaposta; G. Santambrogio; L. Wöste; J. Sauer. *J. Chem. Phys.* 2004, **120**, 6461.

18 G. Santambrogio; M. Brümmer; L. Wöste; J. Döbler; M. Sierka; J. Sauer; G. Meijer; K. R. Asmis. *Phys. Chem. Chem. Phys.* 2008, **10**, 3992; K. R. Asmis; J. Sauer. *Mass Spectrom. Rev.* 2007, **26**, 542.

19 A. P. Scott; L. Radom. *J. Phys. Chem.* 1996, **100**, 16502.

20 G. V. Chertihin; L. Andrews. *J. Phys. Chem. A* 1997, **101**, 8547; R. M. Gordon; A. J. Merer. *Can. J. of Phys.* 1980, **58**, 642; A. J. Merer. *Annu. Rev. Phys. Chem.* 1989, **40**, 407; Y. Gong; M. Zhou; L. Andrews. *Chem. Rev.* 2009, **109**, 6765; *NIST Chemistry WebBook, NIST Standard Reference Database Number 69*; National Institute of Standards and Technology: Gaithersburg MD; Vol. http://webbook.nist.gov; Y. Gong; G. Wang; M. Zhou. *J. Phys. Chem. A* 2008, **112**, 4936.

21 K. Koyama; S. Kudoh; K. Miyajima; F. Mafuné. *J. Phys. Chem. A* 2015, **119**, 8433.

22 P. J. Ziemann; J. A. W. Castleman. *Phys. Rev. B* 1992, **46**, 13480.

23 S. Mauthe; I. Fleischer; T. M. Bernhardt; S. M. Lang; R. N. Barnett; U. Landman. *Angew. Chem. Int. Ed.* 2019, **131**, 8592

24 S. M. Lang; I. Fleischer; T. M. Bernhardt; R. N. Barnett; U. Landman. *Nano Lett.* 2013, **13**, 5549.

25 S. K. Nayak; P. Jena. *Phys. Rev. Lett.* 1998, **81**, 2970; S. K. Nayak; P. Jena. *J. Am. Chem. Soc.* 1999, **121**, 644; H. Kino; L. K. Wagner; L. Mitas. *J. Comput. Theor. Nanosci.* 2009, **6**, 2583.

26 E. Sanville; S. D. Kenny; R. Smith; G. Henkelman. *J. Comput. Chem.* 2007, **28**, 899; W. Tang; E. Sanville; G. Henkelman. *J. Phys.: Cond. Mat.* 2009, **21**, 084204; M. Yu; D. R. Trinkle. *J. Chem. Phys.* 2011, **134**, 064111.

27 E. A. Carter; W. A. Goddard. *J. Phys. Chem.* 1988, **92**, 2109.

28 A. Fernando; T. Haddock; C. M. Aikens. *J. Phys. Chem. A* 2016, **120**, 2480−2492.

29 T. K. Das; M. Couture; Y. Ouellet; M. Guertin; D. L. Rousseau. *PNAS* 2001, **98**, 479; Huber; Herzberg *Molecular Spectra and Molecular Structure Constants of Diatomic Molecules*; Van Nostrand, New York, 1979.

30 C. Lee; C. M. Aikens. *Comp. Theo. Chem.* 2013, **1013**, 32.

31 C. van Dijk. Structure and magnetism of atomic clusters, PhD thesis, Radboud University Nijmegen, 2011.